# Using the Earth as a Polarized Electron Source to Search for Long-Range Spin-Spin Interactions

Larry Hunter *et al.*

*Science* **339**, 928 (2013);
DOI: 10.1126/science.1227460

# Using the Earth as a Polarized Electron Source to Search for Long-Range Spin-Spin Interactions

Larry Hunter,[1]* Joel Gordon,[1] Stephen Peck,[1] Daniel Ang,[1] Jung-Fu Lin[2]

Many particle-physics models that extend the standard model predict the existence of long-range spin-spin interactions. We propose an approach that uses the Earth as a polarized spin source to investigate these interactions. Using recent deep-Earth geophysics and geochemistry results, we create a comprehensive map of electron polarization within the Earth induced by the geomagnetic field. We examine possible long-range interactions between these spin-polarized geoelectrons and the spin-polarized electrons and nucleons in three laboratory experiments. By combining our model and the results from these experiments, we establish bounds on torsion gravity and possible long-range spin-spin forces associated with the virtual exchange of either spin-one axial bosons or unparticles.

Advances in particle physics have contributed to our understanding of the deep Earth, most recently through the observation of geoneutrinos (*1*). By contrast, the contributions to particle physics resulting from our understanding of the Earth have largely been limited to gravitational interactions or using the Earth as a large mass or baryonic source. Here we suggest that our knowledge of the magnetic fields and electron-spin behavior within the Earth is sufficiently developed that we can use the Earth's polarized electrons to study anomalous long-range spin-spin interactions.

Many extensions of the standard model of particle physics predict the existence of new particles. The virtual exchange of these particles between ordinary fermions can result in spin-spin interactions that look quite different from those expected from electromagnetism. The spin-dependent forces that result from the exchange of a pseudoscalar boson like the axion were originally investigated by Moody and Wilczek (*2*). The exchange of a vector boson with mass $m_{z'}$ can lead to the "spin-dot-spin" and "spin-cross-spin" potentials (*3*)

$$V_1 = \frac{g_A^1 g_A^2}{4\pi r}(\hat{\sigma}_1 \cdot \hat{\sigma}_2)e^{-r/\lambda} \qquad (1)$$

$$V_2 = \frac{\hbar^2}{4\pi}\left(\frac{g_V^1 g_A^2}{2M_1} + \frac{g_A^1 g_V^2}{2M_2}\right)(\hat{\sigma}_1 \times \hat{\sigma}_2)\cdot\hat{r}\left(1+\frac{r}{\lambda}\right) \times \left(\frac{1}{r^2}\right)e^{-r/\lambda} \qquad (2)$$

where $g$ denotes the vector (V) or axial (A) coupling constants of fermions 1 or 2 with mass $M$ and spin directions, $\hat{\sigma}$. The interaction range of the force is denoted by $\lambda = \hbar/m_{z'}c$ where $\hbar$ is Planck's constant ($h$) divided by $2\pi$ and $c$ is the speed of light.

Another interesting entity that could produce long-range spin-spin interactions is the "unparticle" (*4*). Unlike ordinary particles, unparticles do not have well-defined masses but can be characterized in terms of an energy scale $\Lambda$, a scaling dimension $d$, and a dimensionless coupling constant $c_A$. In the long-range limit, the virtual exchange of an axial-vector unparticle results in an effective potential (*5*)

$$V_u = -c_A^2 \frac{4\sqrt{\pi}\Gamma(d+1/2)\Gamma(2(d-1))}{(2\pi)^{2d}\Gamma(d-1)\Gamma(2d)}(\hat{\sigma}_1 \cdot \hat{\sigma}_2) \times \left(\frac{\hbar c}{r}\right)\left(\frac{\lambda_u}{r}\right)^{2d-2} \qquad (3)$$

where $\Gamma$ is the gamma function, and $\lambda_u = \hbar c/\Lambda$ is the characteristic length associated with the unparticle. The unparticle potential does not exhibit the usual exponential decay with distance that is associated with the exchange of ordinary massive particles.

Ramsey conducted the first experiment that looked for anomalous spin-spin couplings (*6*). Early work in the field placed limits on such couplings between electrons ($e^-$-$e^-$) (*7, 8*) and between electrons and nucleons (*9*). Recently, constraints have been placed on short-range (atomic scale) anomalous spin-spin forces by considering hyperfine structure in hydrogen-like atoms (*10*), spin-exchange collisions (*11*), and magnetic resonance in deuterated molecular hydrogen (*12*). New searches for long-range interactions have been quite successful in placing bounds on the coupling constants associated with the potentials discussed above. Neutron-neutron ($n$-$n$) spin couplings have been investigated by using nuclear-spin magnetometers with spin-polarized $^3$He used as a source (*13, 14*), whereas the $e^-$-$e^-$ spin interactions have been investigated by using a spin-polarized torsion pendulum with $SmCo_5$-Alnico toroids as sources (*15*). To search for long-range ($\lambda > \sim 1$ m) spin-spin interactions, the polarized source is placed near the apparatus and the direction of its polarization is altered. The spin associated with optically pumped nuclear sources can be reversed simply by changing the circular polarization of the pumping radiation. The solid-state electron-spin sources can be easily rotated in the laboratory. One then looks for a response in the magnetometer or torsion pendulum that is synchronous with the source modulation. Great efforts are made in these experiments to minimize the ordinary magnetic-dipole coupling between the source and apparatus.

**The concept of the experiment.** Here we suggest an alternative approach where, instead of the modulated laboratory spin source, one uses the polarized electrons within the Earth. The advantage of this approach is simply one of numbers. There are $\sim 10^{49}$ unpaired electron spins in the Earth. On average, about one extra electron out of every 10 million will become polarized antiparallel to Earth's magnetic field. Hence, there are on the order of $10^{42}$ polarized electrons in the Earth, compared with $\sim 10^{22}$ polarized neutrons or $\sim 10^{25}$ polarized electrons in a typical laboratory source. Hence, the number of polarized geoelectrons exceeds the number in a laboratory source by a factor of at least $10^{17}$. Laboratory sources are usually located a few tenths of a meter from the detection apparatus while a typical geoelectron is a few thousand kilometers away. For ordinary electromagnetism and for the spin-spin potentials associated with pseudoscalar bosons, the dipole-dipole interaction falls off as the cube of the distance, $r$, and the increased distance of the geoelectrons reduces the interaction potential by ~21 orders of magnitude. For such potentials there is no net advantage in considering an Earth source. However, many of the anomalous spin-spin potentials (e.g., Eqs. 1 to 3) fall off as $1/r^n$, where $n$ is between 1 and 2. For these potentials, the suppression of the sensitivity by the distance will be between 7 and 14 orders of magnitude. Here, even with additional losses due to poor geometry and lower experimental sensitivity, a geoelectron source can result in substantially improved constraints.

The greatest disadvantage to searching for spin interactions with the Earth is that one cannot modulate the spin source. To extract the geoelectron spin-spin signal, one must reverse or modulate the contribution it makes to the experimental signal. This can be accomplished by mounting the detection apparatus on a rotating table. Such systems have been developed for searches for violations of local Lorentz invariance (LLI) (*16, 17*). Although most contributions to the experimental signal are independent

[1]Physics Department, Amherst College, Amherst, MA 01002, USA. [2]Department of Geological Sciences, Jackson School of Geosciences, The University of Texas at Austin, Austin, TX 78712, USA.

*To whom correspondence should be addressed. E-mail: lrhunter@amherst.edu

of the table orientation, the "effective" spin associated with the geoelectrons creates a preferred axis in the laboratory that couples to the table position via the various spin-spin interactions (Eqs. 1 to 3).

**Energy bounds on spins oriented relative to Earth.** We use the measurements reported from two recent LLI experiments [one in Amherst, MA ($\theta_{lat}$ = 42.37°N, 72.53°W) (*18*) and another in Seattle, WA (47.658°N, 122.3°W) (*19*)], and bounds from an earlier Seattle experiment that searched for the coupling of nuclear spin to Earth's gravitational field (*20*), to extract limits on the associated spin-spin couplings.

The geometry of the Amherst $^{199}$Hg-Cs comagnetometer experiment is shown in Fig. 1. The experiment is mounted on a table that rotates between two data-collection positions separated by 180°. The table rotation changes the direction of the applied magnetic field vector from $\mathbf{B}_{app1}$ to $\mathbf{B}_{app2}$. This inverts the horizontal component of the magnetic field while leaving the vertical component fixed. The Cs magnetometer is used to hold the magnitude of the magnetic field constant. The change in the $^{199}$Hg nuclear precession frequency with the table position is measured to be $\Delta\nu_N^{Hg} < 1.1\,\mu$Hz ($2\sigma$ bounds will be quoted throughout this paper). The resulting bound on the energy of a $^{199}$Hg nuclear spin ($\hat{\sigma}_1$ in Fig. 1) oriented north (N) is $\beta_N^{Hg} < h\Delta\nu_N^{Hg}/(4\sin\theta_B) = 1.3\times10^{-21}$ eV, where the geometric factor is associated with the magnetic field angle with respect to vertical ($\theta_B$ = 63.8°) and the factor of 4 accounts for the differences between the two table positions and the two orientations of the nuclear spin with respect to the applied field. We follow the notation of (*19*) in using a "hat" over β to indicate that a correction for Earth's gyroscopic frequency has been applied. A random geoelectron with a spin $\hat{\sigma}_2$, separated from the apparatus by a distance *r*, is also shown in the plot. To place bounds on the coupling strengths in Eqs. 1 and 3, we sum the interaction potentials over all of Earth's spin-polarized electrons and require that the resulting energy not exceed $\hat{\beta}_N^{Hg}$.

The coupling of the geoelectron spins by the spin-cross-spin potential (Eq. 2) is about an order of magnitude larger for detection spins oriented east (E) than for those oriented north. To improve our bounds on this potential, we have made additional measurements with our apparatus (*18*) rotated 90°. In this orientation, the horizontal component of the applied magnetic field changes from east to west when the table changes position. We measure the change in the $^{199}$Hg nuclear precession frequency with the table position to be $\Delta\nu_E^{Hg} < 0.8\,\mu$Hz. The resulting bound on the energy of a $^{199}$Hg nuclear spin oriented east is $\beta_E^{Hg} < h\Delta\nu_E^{Hg}/(4\times\sin(63.8°)) = 9\times10^{-22}$ eV. We use this bound to constrain the strength of the spin-cross-spin potential.

In their search for a cosmic preferred frame, a recent Seattle experiment constrains possible directional couplings to the polarized electrons that make up their $SmCo_5$-Alnico torsion pendulum. Their bounds on a spin potential coupling electron spin along the north and east directions are $\hat{\beta}_N < 5.9\times10^{-21}$ eV and $\hat{\beta}_E < 8\times10^{-22}$ eV. Both of these bounds can be used to set limits on electron-electron spin-spin couplings of Eqs. 1 to 3. In practice, the superior experimental bound along the east direction yields the best electron limits on all three potentials.

The third experiment that we have considered was explicitly designed to search for a coupling between local gravity and nuclear spin. The experiment compares the precession frequencies of $^{199}$Hg and $^{201}$Hg in a comagnetometer arrangement. This experiment is not mounted on a rotating table, but instead modulates the detection by periodically reversing the direction of the applied magnetic field and occasionally inverting the orientation of the apparatus. Unlike the LLI experiments, where the sensitive directions lie in the horizontal plane, the magnetometer field is oriented along Earth's spin axis (*z*). Using an updated nuclear structure calculation (*21*), the experiment places a bound on the neutron (*n*) and proton (*p*) spin couplings along the *z* axis, $\hat{B}_z^n < \frac{1}{2}(3.6\times10^{-20}\text{ eV})\cos(47.5°) = 1.2\times10^{-20}$ eV and $\hat{B}_z^p < \frac{1}{2}(5.2\times10^{-20}\text{ eV})\cos(47.5°) = 1.8\times10^{-20}$ eV. Here the geometrical factor transforms the bound from along the vertical to along *z* and the factor of 2 accounts for the two orientations of the nuclear spins with respect to the applied field.

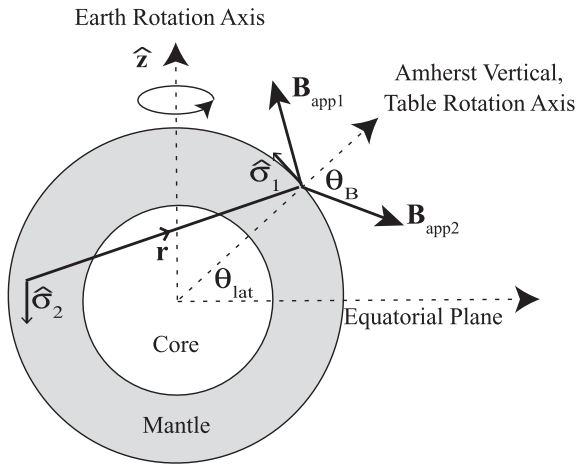


**Fig. 1.** The geometry of the Amherst experiment (see text for explanation).

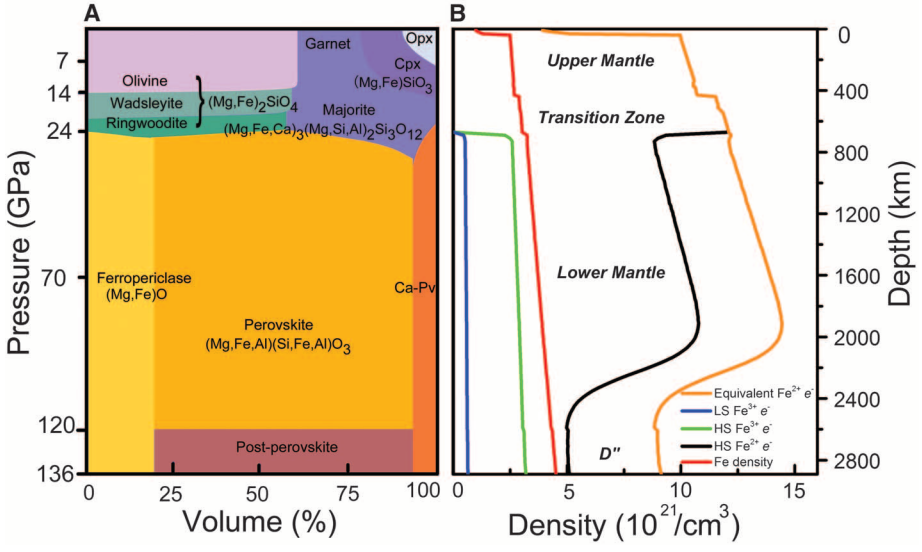


**Fig. 2.** (**A**) Mineral proportions in the pyrolite model as a function of depth and (**B**) the resulting iron and electron densities in the various electronic spin states. The PREM model pressure profile is used throughout the calculations (*30*). The volume fractions and the iron fractions of the mantle are from (*23*), while the densities and iron fractions for the crust are from (*28*). The "Equivalent $Fe^{2+}$ $e^-$" density combines the electrons in the different spin states, weighted by a factor that takes into account the relevant proportion of their contribution to the polarized electron-spin density. For the *D″* layer with the silicate post-perovskite phase between the core and the mantle, we use the temperature gradient suggested in (*29*).

**Electron-spin density map.** To use Earth as a spin source requires creating a map of the polarized electron-spin density and direction everywhere within the Earth. Three input parameters are needed to create this map: temperature, direction and magnitude of Earth's magnetic field, and the density of unpaired electrons that can be aligned in the external field. We consider each of these in the following discussion.

Earth's core is mostly made of metallic Fe with ~5% Ni, together with some lighter elements. First-principles calculations indicate that there is no paramagnetism associated with the Fe-Ni alloy in the core (*22*). Hence, the core makes no contribution to Earth's polarized spin density and will be neglected in our model.

The electron-spin density in Earth's mantle can be calculated by using recent results from deep-Earth mineral physics, geochemistry, and seismology. The volume fractions and iron contents of various regions of the mantle have been reported experimentally (Fig. 2) (*23*). Because we are interested in establishing upper bounds on the spin-spin coupling constants, we shall make a conservative estimate of the magnitude of the electronic spins within the Earth. Iron, the most abundant transition metal in oxides and silicates of Earth's mantle and crust, has a partially filled d-shell that dominates the resulting paramagnetism of the mantle minerals and crustal rocks. Other major rock-forming elements such as Mg, Si, Al, and O with closed electron shells have negligible contributions to the polarized spin density. We use a representative pyrolite compositional model of the mantle that assumes there is no major chemical difference between the elemental composition of the upper and lower mantle (*24*). Alternative models generally yield higher iron concentrations in the lower mantle (*25*). We use the Birch-Murnaghan equation of state (*26*), relevant physical parameters of the mantle silicates and oxides, and expected pressure-temperature profiles of the crust and mantle (geotherm) to calculate the densities of the major mantle minerals at different depths (see table S1 for details) (*27*–*29*). In fig. S1, we compare our calculated mean density of these minerals at various depths with the seismic preliminary reference Earth model (PREM) values (*30*).

Most of the iron in Earth's crust and mantle is bound up in mineral lattices with either ferrous ($Fe^{2+}$) or ferric ($Fe^{3+}$) valence states. For the crust and upper mantle, most of the iron exists in the $Fe^{2+}$ state with four unpaired d-shell electrons and a total spin $S = 2$, the so-called high-spin (HS) state. The lower mantle has two primary iron-bearing constituents, ferropericlase (fp) and perovskite (pv), whereas silicate post-perovskite (ppv) likely exists in the lowermost mantle (the D″ region) (Fig. 2). Ferropericlase consists predominantly of ferrous iron while pv and ppv consist of approximately half $Fe^{2+}$ and half $Fe^{3+}$. In the lower mantle, fp undergoes a transition from its HS state to a low-spin (LS) state with $S = 0$ (*31*). Along an expected lower-mantle geotherm (*32*), experimental results show that the spin crossover of $Fe^{2+}$ in fp starts at ~70 GPa (1700-km depth) and 2200 K and completes at ~125 GPa (2700-km depth) and 2400 K (*33*). This spin crossover reduces the unpaired electron density at depths greater than ~2100 km (Fig. 2). The spin states of iron in pv and ppv remain under debate, but the current consensus is that a similar spin transition from $S = 5/2$ to $S = 1/2$ is expected to occur in $Fe^{3+}$ in the octahedral site (B site) of pv and ppv whereas $Fe^{2+}$ remains in the HS state at all mantle pressures (*34*). We choose again to conservatively assume that all of the $Fe^{3+}$ in the B site of pv and ppv, which is ~25% of all iron in those minerals, is in the LS state, whereas the remainder of the $Fe^{3+}$ and $Fe^{2+}$ remains in the HS states. The resulting unpaired electron densities as a function of depth are shown in Fig. 2.

For our model to be successful, the magnitude and direction of Earth's magnetic field, **B**, must be known everywhere between the core and the surface. The magnetic field within the Earth is predominantly created by electrical currents within the core (*35*). We use the world magnetic model (WMM 2010) (*36*) to recreate the magnetic field within the Earth as it existed when the data were collected. The magnetic field is derived from a magnetic potential that is approximated by a 12th-order associated Legendre expansion. The coefficients of the expansion are chosen to yield a best fit to worldwide and satellite observations. The model is expected to be valid throughout the mantle and crust, where the material is believed to be electrically insulating. For the Amherst data, we model the field as it was on 1 October 2010, while for the Seattle data we use 1 July 2007 for the torsion pendulum experiment and 1 January 1991 for the Hg comagnetometer experiment. In practice, Earth's magnetic variation is sufficiently slow that altering the chosen date by a decade does not produce any notable change in our results.

When an iron ion in the mantle interacts with this external field, the spin becomes slightly polarized. We assume that the orbital moments are quenched and can be neglected. The average value of the spin of each HS $Fe^{2+}$ (in units of $\hbar$) along the magnetic field is $\langle S_z \rangle_{Iron} = 2g\mu_B B/k_B T$, where $\mu_B$ is the Bohr magneton, $k_B$ is Boltzmann's constant, $T$ is the temperature, and $g$ is the electron $g$ factor. Because on average, each of the four unpaired electrons has a projection of its spin along $z$ that is ¼ of that for the lattice site, the effective alignment of each electron in the

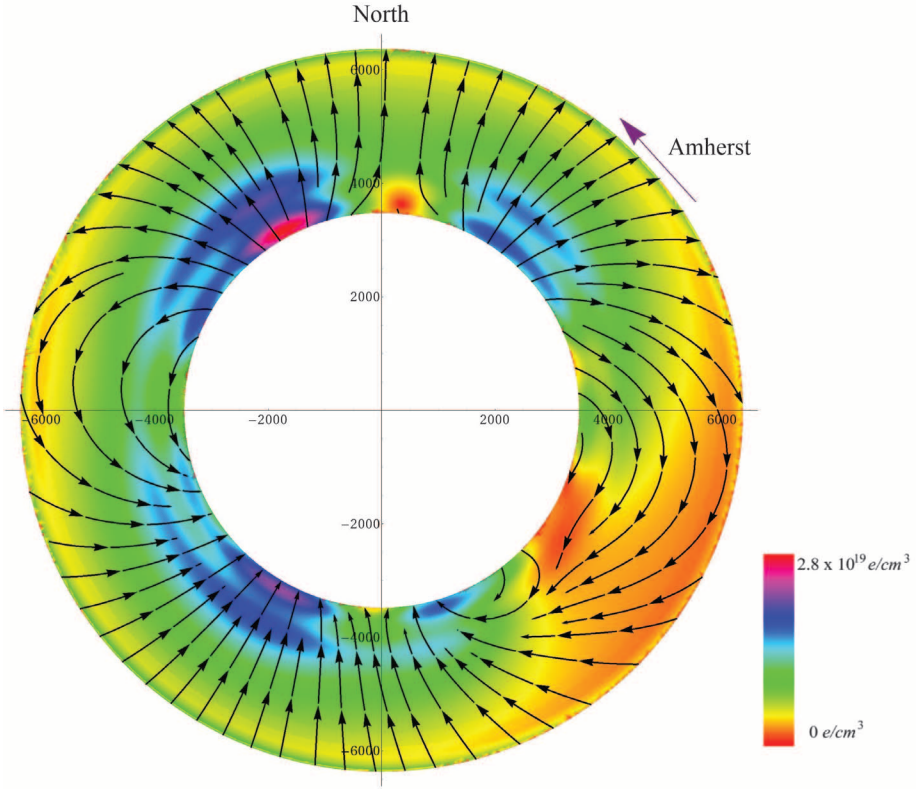


**Fig. 3.** The polarized electron-spin density on a plane that contains Earth's rotation axis and Amherst, MA. The black arrows indicate only the direction of the electron spins, while the color shading of the plot indicates the magnitude of the polarized electron-spin density. The density of the arrows on the plot is not meaningful. The $\hat{\phi}$ (east) component of the field (into or out of the page) is not shown. The electron-spin density within the core (white central circle) is assumed to be zero. The violet vector corresponds to the north orientation and location of the Amherst apparatus. The vertical $z$ axis is along Earth's rotation axis, and the axis labels have units of kilometers.

external field is $\langle S_z \rangle_e = g\mu_B B/2k_B T$. For a spin ½ electron in HS $Fe^{2+}$, this corresponds to an average spin alignment of $2\mu_B B/k_B T$, where we assume $g = 2$. Similar considerations for the LS ($S = 1/2$) and HS ($S = 5/2$) states of $Fe^{3+}$ yield average electron spin alignments of $\mu_B B/k_B T$ and $7\mu_B B/3k_B T$, respectively (*37*). Figure 1 shows the "equivalent $Fe^{2+}$ $e^-$" density, where we have taken this weighting into account. The polarized electron-spin density is determined by simply multiplying this density by $2\mu_B B/k_B T$. For a field of 1 G and a temperature of 2000 K, a typical HS $Fe^{2+}$ electron's polarization is about $7 \times 10^{-8}$.

Combining the magnetic field map with the temperature and electron-spin density profiles yields a map of the polarized electron-spin density and direction within the Earth. A sampling of the result on a plane that includes Earth's rotation axis and Amherst is shown in Fig. 3. The general rise in the magnitude of the polarization with decreasing radius is due to the increased magnitude of the magnetic field and the higher density of the constituent minerals. When moving in toward the core, the abrupt drop in the polarized spin density at a radius of about 4200 km is associated with the spin transition in fp, whereas the drop just before reaching the core is a result of the rising temperature. The slight rise in the spin density at the crust is associated with the rapidly decreasing temperature as one approaches the surface. The reduction of the spin density in the fourth quadrant of the plot results from a minimum in the Earth field commonly referred to as the South Atlantic Anomaly (*38*). Also shown on the plot is a vector corresponding to the north orientation of the Amherst apparatus ($\hat{\sigma}_1$ in Fig. 1). In this orientation, only geoelectron spin components parallel to this direction contribute to the dot product between the source and detection spins (Eqs. 1 and 3). Cross-product contributions (Eq. 2) are maximized when the detector orientation is east, which is into the page at Amherst on Fig. 3.

**Interaction potentials.** With the polarized geoelectron spin density and direction known everywhere within the Earth, we can calculate the interaction potential associated with each of the possible spin interactions described in Eqs. 1 to 3. The various integrations over the Earth volume are run in Mathematica using geocentric coordinates (see fig. S2 for details). For $1/r$ and $1/r^2$ potentials, the relative contributions to the integral from various depths are shown in fig. S3. For the $1/r$ ($1/r^2$) potential, the relative contributions to the integral from the crust, upper mantle, and lower mantle are 2, 31, and 66% (6, 43, and 51%), respectively. To limit couplings between the geoelectrons and $^{199}$Hg nuclei, we require that the integrated spin-spin potentials (relative to Amherst) remain smaller than the observed experimental upper bound: $\hat{\beta}_N^{Hg}$ for the spin-dot-spin potentials (Eqs. 1 and 3) and $\hat{\beta}_E^{Hg}$ for the spin-cross-spin potential (Eq. 2). To extract the bounds on the electron coupling to the neutron and proton, we assume that the $^{199}$Hg nuclear spin has a neutron spin projection of –31% and a proton spin projection of –3% (*21*). The bounds on the electron-electron couplings and additional bounds on the electron-neutron and electron-proton couplings are similarly derived from integrations relative to Seattle and the bounds $\beta_E^e$, $\hat{\beta}_z^n$, and $\hat{\beta}_z^p$. The results for a potential mediated by an intermediate vector boson of mass $m_{z'}$ are shown in Fig. 4. Limits on the unparticle couplings are shown in Table 1.

Our predicted bounds are markedly insensitive to changes in various Earth-model parameters. The bounds in Fig. 4 are proportional to the absolute temperature and inversely proportional to the densities assumed. Hence, a 20% change in either the density or the temperature would change the bounds by about 20%. Such large departures from the pyrolite and PREM values used here seem highly unlikely. Indeed, Amherst should be reasonably well represented by the average continental values assumed. Seattle resides on top of a deep, ancient subducting plate that may produce appreciable local cooling (*39*). However, lower temperatures would only further improve the bounds obtained from the model. We do not report any limits from our model for ranges less than 1 km where local density variations and the possibilities of local ferromagnetic materials render the results unreliable. On the logarithmic plots of Fig. 4, a 20% change would result in a shift that is less than the thickness of the plotted lines.

**Discussion.** Our results establish limits on many of the possible long-range spin-spin interactions between fermions. For the axial-axial exchange (Eq. 1), the low-mass limits achieved are about a million times lower than the *n-n* limits that were established with a laboratory source. In the long-range limit, the potential has the same $1/r$ dependence as gravity, and one can calculate the ratio between the strength of the spin-spin coupling between two particles to their gravitational

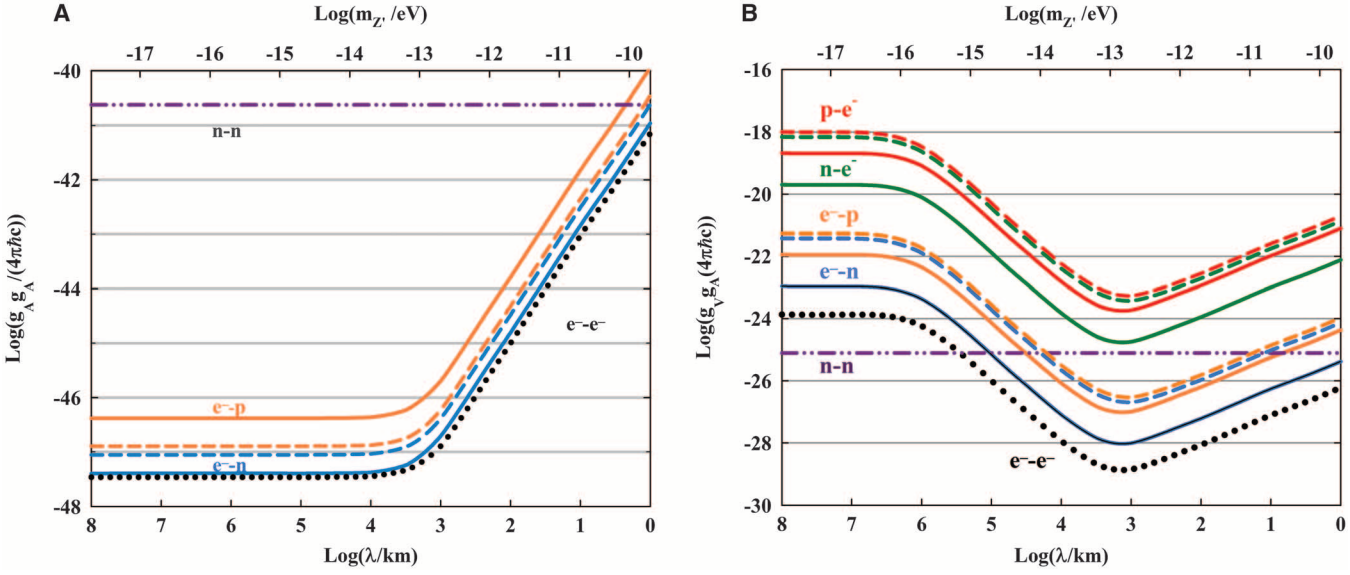


**Fig. 4.** (**A**) Bounds on the long-range axial-axial couplings (Eq. 1) as a function of the range and mass of the intermediate vector boson. All regions of the plots above the lines are excluded. The violet lines (mixed dots and dashes) are the *n-n* bound established by (*13*). All other bounds are from the present analysis. We extract the $e^-$-$e^-$ bounds (black dots) from the data in (*19*) and the $e^-$-*p* (orange) and $e^-$-*n* (blue) bounds from the data in (*18*) (solid lines) and (*20*) (dashed lines). (**B**) Bounds on the vector (V)–axial (A) couplings (Eq. 2). The first fermion of each labeled pair has the vector coupling, whereas the second has the axial coupling. The violet and black limits are derived as discussed in (A). We extract the $e^-$-*p* (orange), $e^-$-*n* (blue), *n*-$e^-$ (green), and *p*-$e^-$ (brown) bounds from our new measurement of $\beta_E^{Hg}$ (solid lines) and the data in (*20*) (dashed lines). Here $e^-$, *n*, and *p* correspond to the electron, neutron, and proton.

**Table 1.** Upper bounds on the axial dimensionless coupling $c_A$ associated with unparticles with scaling dimension $d$. Here $e^-$, $n$, and $p$ denote the couplings between electrons, neutrons, and protons. The $n$-$n$ limit was established in (*13*). All other bounds are from the present analysis. We extract the $e^-$-$n$, $e^-$-$p$, and $e^-$-$e^-$ bounds from the data in (*18*), (*20*), and (*19*), respectively. For ease of comparison with the $n$-$n$ results, we have set $\Lambda = 1$ TeV in this analysis.

| $c_A$\|$d$ | 1 | 1.125 | 1.25 | 1.33 | 1.375 | 1.5 |
|---|---|---|---|---|---|---|
| $e^-$-$n$ | $7 \times 10^{-24}$ | $1 \times 10^{-20}$ | $2 \times 10^{-17}$ | $2 \times 10^{-15}$ | $3 \times 10^{-14}$ | $6 \times 10^{-11}$ |
| $e^-$-$p$ | $1 \times 10^{-23}$ | $2 \times 10^{-20}$ | $4 \times 10^{-17}$ | $4 \times 10^{-15}$ | $6 \times 10^{-14}$ | $1 \times 10^{-10}$ |
| $e^-$-$e^-$ | $7 \times 10^{-24}$ | $1 \times 10^{-20}$ | $2 \times 10^{-17}$ | $2 \times 10^{-15}$ | $3 \times 10^{-14}$ | $5 \times 10^{-11}$ |
| $n$-$n$ | $1 \times 10^{-20}$ | | $1 \times 10^{-15}$ | $4 \times 10^{-14}$ | | $8 \times 10^{-11}$ |

attraction. Our bounds imply that this ratio is <0.2% for $e^-$-$e^-$ interactions and $<1.2 \times 10^{-6}$ for $e^-$-$n$ interactions. Quantum gravity can induce an effective four-fermion axial interaction with a characteristic coupling of $M_1 M_2 M_p^2$ where $M_1$ and $M_2$ are the fermion masses and $M_p \approx 1.2 \times 10^{-19}$ GeV/$c^2$ is the Planck mass (*40*–*42*). For two electrons, this yields a dimensionless coupling of $10^{-45}$, whereas for a neutron and an electron the characteristic coupling is $10^{-42}$. Our measured long-range bounds on these couplings (Fig. 3) are less than $10^{-47}$, suggesting that our results could be sensitive to such quantum gravity effects.

For the vector-axial coupling of the spin-cross-spin potential (Eq. 2), the range dependence of the limits is more complex. Our limits improve on the bounds obtained by laboratory sources (by as much as a factor of 4000) but only for ranges, ~1 km < λ < ~200,000 km. The integration exhibits a high degree of cancellation for ranges significantly larger than Earth's diameter, suggesting a contribution from Earth's more distant hemisphere of opposite sign and nearly equal magnitude to that from the near hemisphere.

For the unparticle exchange with $d = 1$, the potential falls off as $1/r$, and the bounds on the $e^-$-$n$ and $e^-$-$e^-$ coupling amplitudes are more than a thousand times more restrictive than all previous results. Unparticles with $d = 1.5$ correspond to a dot product potential that falls off as $1/r^2$. Here our bounds become similar to those that have been achieved with laboratory sources.

**Outlook.** Because the spins in our apparatus on Earth's surface have a higher eastward velocity than most of the spins within the mantle, the geoelectron source offers the possibility of testing all of the velocity-dependent effective potentials proposed in (*3*). Experiments using laboratory sources are not sensitive to these terms, and most of these possible spin-spin potentials are currently unbounded. Ongoing development of comagnetometers and nuclear gyroscopes (*43*) should result in improved experimental sensitivities that will allow further refinement of the electron-nucleon couplings. With a different set of assumptions, it may be possible to extend this model so that Earth might be used as a source of nuclear spin. This might allow more stringent limits to be established on nucleon-nucleon spin couplings. Performing the experiment in a region where the surface magnetic field is stronger and more parallel to the surface can substantially enhance sensitivity. An identical experiment conducted in southern Thailand would have about twice the sensitivity of one conducted in Amherst.

If refined experiments find evidence for a long-range spin-spin interaction, the discovery could provide a powerful tool for the investigation of the mantle. Once the potential is well understood, measurements similar to those discussed here could be used to probe Earth's iron concentration and its spin and valence states as a function of depth (*31*, *33*). Such information might eventually help reconcile seismic observations and mineral physics data with geochemical models (*23*, *25*, *44*).

### References and Notes


1. A. Gando *et al.*, *Nat. Geosci.* **4**, 647 (2011).
2. J. E. Moody, F. Wilczek, *Phys. Rev. D Part. Fields* **30**, 130 (1984).
3. B. A. Dobrescu, I. Mocioiu, *J. High Energy Phys.* **11**, 005 (2006).
4. H. Georgi, *Phys. Rev. Lett.* **98**, 221601 (2007).
5. Y. Liao, J.-Y. Liu, *Phys. Rev. Lett.* **99**, 191804 (2007).
6. N. F. Ramsey, *Physica* **96A**, 285 (1979).
7. T. C. P. Chui, W.-T. Ni, *Phys. Rev. Lett.* **71**, 3247 (1993).
8. V. F. Bobrakov *et al.*, *JETP Lett.* **53**, 294 (1991).
9. D. J. Wineland, J. J. Bollinger, D. J. Heinzen, W. M. Itano, M. G. Raizen, *Phys. Rev. Lett.* **67**, 1735 (1991).
10. S. G. Karshenboim, *Phys. Rev. A* **83**, 062119 (2011).
11. D. F. Jackson Kimball, A. Boyd, D. Budker, *Phys. Rev. A* **82**, 062714 (2010).
12. M. P. Ledbetter, M. V. Romalis, D. F. Jackson Kimball, Constraints on short-range spin-dependent interactions from scalar spin-spin coupling in deuterated molecular hydrogen. *Phys. Rev. Lett.* **110**, 040402 (2013).
13. G. Vasilakis, J. M. Brown, T. W. Kornack, M. V. Romalis, *Phys. Rev. Lett.* **103**, 261801 (2009).
14. A. G. Glenday, C. E. Cramer, D. F. Phillips, R. L. Walsworth, *Phys. Rev. Lett.* **101**, 261801 (2008).
15. C. E. Cramer, A torsion balance search for spin-coupled forces, thesis, Univ. of Washington (2007).
16. L. S. Hou, W. T. Ni, Y. C. M. Li, *Phys. Rev. Lett.* **90**, 201101 (2003).
17. J. M. Brown, S. J. Smullin, T. W. Kornack, M. V. Romalis, *Phys. Rev. Lett.* **105**, 151604 (2010).
18. S. K. Peck *et al.*, *Phys. Rev. A* **86**, 012109 (2012).
19. B. R. Heckel *et al.*, *Phys. Rev. D Part. Fields Gravit. Cosmol.* **78**, 092006 (2008).
20. B. J. Venema, P. K. Majumder, S. K. Lamoreaux, B. R. Heckel, E. N. Fortson, *Phys. Rev. Lett.* **68**, 135 (1992).
21. V. Flambaum, S. Lambert, M. Pospelov, *Phys. Rev. D Part. Fields Gravit. Cosmol.* **80**, 105021 (2009).
22. D. Alfè, M. J. Gillan, *Phys. Rev. B* **58**, 8248 (1998).
23. T. Irifune *et al.*, *Science* **327**, 193 (2010).
24. A. E. Ringwood, *Geochim. Cosmochim. Acta* **55**, 2083 (1991).
25. R. Jeanloz, E. Knittle, *Philos. Trans. R. Soc. Lond. A* **328**, 377 (1989).
26. F. Birch, *J. Geophys. Res.* **91**, (B5), 4949 (1986).
27. J. P. Poirier, *Introduction to the Physics of the Earth's Interior* (Cambridge Univ. Press, Cambridge, ed. 2, 2000).
28. F. D. Stacey, P. M. Davis, *Physics of the Earth* (Cambridge Univ. Press, Cambridge, ed. 4, 2008).
29. T. Lay, J. Hernlund, B. A. Buffett, *Nat. Geosci.* **1**, 25 (2008).
30. A. M. Dziewonski, D. L. Anderson, *Phys. Earth Planet. Inter.* **25**, 297 (1981).
31. J. F. Lin, T. Tsuchiya, *Phys. Earth Planet. Inter.* **170**, 248 (2008).
32. J. M. Brown, T. J. Shankland, *Geophys. J. R. Astron. Soc.* **66**, 579 (1981).
33. Z. Mao, J. F. Lin, J. Liu, V. B. Prakapenka, *Geophys. Res. Lett.* **38**, L23308 (2011).
34. Y. G. Yu, H. Hsu, M. Cococcioni, R. M. Wentzcovitch, *Earth Planet. Sci. Lett.* **331–332**, 1 (2012).
35. B. A. Buffett, *Science* **288**, 2007 (2000).
36. S. Maus *et al.*, "The US/UK World Magnetic Model for 2010-2015" (National Oceanic and Atmospheric Administration, Technical Report NESDros. Inf. Serv./NGDC 2010).
37. C. Kittel, *Introduction to Solid State Physics* (Wiley, ed. 5, 1976).
38. G. Hulot, N. Olsen, T. J. Sabaka, in *Treatise Geophys.*, G. Schubert, Ed. (Elsevier, Amsterdam, 2007), vol. 5, chap. 33.
39. Y. Tian, D. Zhao, *Phys. Earth Planet. Inter.* **200–201**, 72 (2012).
40. D. E. Neville, *Phys. Rev. D Part. Fields* **25**, 573 (1982).
41. T. W. B. Kibble, *J. Math. Phys.* **2**, 212 (1961).
42. I. B. Khriplovich, *Phys. Lett. B* **709**, 111 (2012).
43. E. A. Donley, J. Kitching, Nuclear Magnetic Resonance Gyroscopes in *Optical Magnetometry*, D. Budker, D. F. Jackson-Kimball, Eds. (Cambridge Univ. Press, Cambridge, 2012).
44. M. Murakami, Y. Ohishi, N. Hirao, K. Hirose, *Nature* **485**, 90 (2012).



**Acknowledgments:** We thank S. Maus, R. Jeanloz, B. Buffett, W. Loinaz, and P. Crowley for useful conversations. We thank A. Anderson, D. Hanneke, and N. Bern for computational and graphics assistance, and C. Lu and J. Yang for compiling mineral physics data and helping with Fig. 2, respectively. We thank N. Fortson and B. Heckel for providing the updated neutron and proton bounds from (*20*). We thank the editors and reviewers for constructive suggestions. This work was supported by funds from the Amherst College Dean of Faculty and the NSF under grants PHY-0855465 and PHY-1205824. J.-F.L acknowledges support from the U.S. NSF (EAR-1056670 and EAR-1053446), Energy Frontier Research in Extreme Environments (EFree), and the Carnegie/DOE Alliance Center (CDAC). The data presented here are available on request from lrhunter@amherst.edu.


### Supplementary Materials

www.sciencemag.org/cgi/content/full/339/6122/928/DC1
Figs. S1 to S3
Table S1
References (*45*–*50*)

16 July 2012; accepted 26 December 2012
10.1126/science.1227460